

**Advanced Diffusion Imaging:
Fast/Slow Diffusion, HARDI, DSI, and White Matter Tractography**
Andrew L. Alexander, Ph.D., Yu-Chien Wu, M.D., M.S., Mariana Lazar, Ph.D.
Department of Medical Physics, Waisman Laboratory for Brain Imaging and Behavior,
University of Wisconsin – Madison

Effects of Large Diffusion-Weighting: Measurements of water diffusion using MRI may be used to study the architecture (geometry and order) of tissue microstructure. The diffusion tensor is a relatively simple and elegant model of water diffusion [1]. This model assumes that the distribution of diffusion displacements ($\mathbf{R} = \mathbf{R}_1\text{-}\mathbf{R}_2$) for a given diffusion time, Δ , is Gaussian,

$$P(\mathbf{R}, \Delta) = \frac{1}{\sqrt{(4\pi\Delta)^3 |\mathbf{D}|}} \exp\left\{-\frac{\mathbf{R}^T \mathbf{D}^{-1} \mathbf{R}}{4\Delta}\right\}, \quad (1)$$

which results in a mono-exponential decay with diffusion-weighting

$$S = S_0 e^{-b\hat{\mathbf{g}}^T \mathbf{D} \hat{\mathbf{g}}}, \quad (2)$$

where \mathbf{D} is the diffusion tensor, $\hat{\mathbf{g}}$ is the unit vector describing the gradient orientation, S_0 is the signal without diffusion weighting, and b is the amount of diffusion weighting.

The diffusion tensor is a good model of the diffusion-weighted signal behavior for low levels of diffusion weighting (e.g., $b < 1500$ s/mm²). However, the diffusion tensor model does not appear to be consistently accurate in describing the signal behavior for higher levels of diffusion-weighting (e.g., $b > 2000$ s/mm²). The problems with the simple diffusion tensor model arise from two sources – (1) apparent “fast” and “slow” diffusing components [2,3] that cause the signal decay with diffusion-weighting to appear bi-exponential; and (2) partial volume averaging [4] between tissue groups with distinct diffusion tensor properties (e.g., crossing white matter (WM) tracts, averaging between WM and gray matter tissues). The fast and slow diffusion signals are likely to arise from local restriction effects from cellular membranes although some have hypothesized that these signals correspond to intra- and extra-cellular diffusion.

The effect of partial volume averaging causes ambiguities in the interpretation of diffusion tensor measurements. Whereas the diffusion anisotropy is generally assumed to be high in white matter, regions of crossing white matter tracts will have artifactually low diffusion anisotropy. Consequently, in regions with complex white matter organization, changes or differences in diffusion tensor measures may reflect either changes in either the tissue microstructure or the partial volume averaging components. As the diffusion-weighting is increased the profiles of apparent diffusivity reveal non-Gaussian diffusion behavior in voxels with partial volume averaging.

A growing number of strategies have been developed for measuring and interpreting complex diffusion behavior (see Table 1). The methods vary in their acquisition sampling and analysis approaches. For all of the approaches described here, increasing the maximum diffusion-weighting will improve the characterization of both the slow diffusion components and the partial volume effects, although the measurement SNR will be decreased.

Table 1. Methods for High DW Diffusion Imaging

| Technique | Full Name | Refs | Description | ~ N_e |
|-----------|---|--------|--|-----------------------|
| BEDI | Bi-Exponential Diffusion Imaging | 2,3 | Bi-exponential model of DW signal | 16 - 60 |
| MDTI | Multiple DTI | 5,6 | Two tensor model – fast/slow diffusion | 70-192. |
| DSI | Diffusion Spectrum Imaging | 12, 13 | Empirical model-free estimation of diffusion displacements using q-space | Typically $N_e > 400$ |
| HARDI | High Angular Resolution Diffusion Imaging | 7,8 | Estimate ADC profile versus encoding angle | 43 - 60 |
| GDTI | Generalized DTI | 9,10 | Higher order tensor model of HARDI data | 81-200 |
| QBI | q-Ball Imaging | 11 | Estimation of displacement distribution based upon HARDI data | 253 |
| CHARMED | Combined Hindered and Restricted Model of Diffusion | 14 | q-space derived model of hindered and restricted (fast/slow) diffusion | 169 |
| HYDI | Hybrid Diffusion Imaging | 15 | Estimates DTI, DSI, and QBI w/ non-uniform q-space sampling | 100-250 |

Fast/Slow Diffusion Modeling: Diffusion-weighted measurements over a range of diffusion-weighting have been used to estimate apparent fast and slow components of both apparent diffusivities (BEDI: bi-exponential diffusion imaging) and diffusion tensors (MDTI: multiple diffusion tensor imaging) [2,5,6]. In these cases, the measurements are fit to

$$S = S_0 \left(k e^{-b\hat{g}^T \mathbf{D}_f \hat{g}} + (1-k) e^{-b\hat{g}^T \mathbf{D}_s \hat{g}} \right) \quad (3)$$

where \mathbf{D}_f and \mathbf{D}_s are the fast and slow diffusion tensors, and k is the signal fraction from the fast compartment. For a fixed diffusion encoding direction, the signal decay appears bi-exponential with diffusion-weighting. Bi-exponential strategies are appropriate for the cases where there is no significant partial voluming expected and when the diffusion may be modeled using a combination of narrow and broad Gaussian distributions. As discussed earlier, partial volume effects (e.g., crossing WM fibers) will significantly complicate the interpretation of fast and slow diffusing components. In addition, the assignment of these components has been controversial.

High Angular Resolution Diffusion Imaging (HARDI): In order to better characterize the angular diffusion features associated with crossing white matter tracts, several diffusion encoding approaches have been developed that use a large number of encoding directions ($N_e > 40$ up to several hundred) at a fixed level of diffusion-weighting [7,8]. Although HARDI studies have been reported with diffusion-weighting as low as $b = 1000 \text{ s/mm}^2$ [7], the separation of tract components will be much better for higher diffusion-weighting. The original HARDI methods [7,8] estimated the profiles of apparent diffusion coefficients and used spherical harmonic decomposition methods to estimate the complexity of the diffusion profiles

$$D(\theta, \phi) = \sum_{l=0}^{\infty} \sum_{m=-l}^l a_{lm} Y_{lm}(\theta, \phi) \quad \text{where} \quad a_{lm} = \iint_{0}^{2\pi} \iint_{0}^{\pi} D(\theta, \phi) Y_{lm}^*(\theta, \phi) \sin\theta d\theta d\phi \quad (4)$$

where Y are the spherical harmonic basis functions, $*$ denotes complex conjugate, and a are the coefficients. Higher order spherical harmonic basis functions represent signal terms that may correspond to crossing white matter tracts in the voxel. The indices l and m refer to the order and degree of the spherical harmonic basis, where $l = 0$ is isotropic, $l = 2$ is a single fiber, $l = 4$ are 2 fiber groups and $l = 6$ are 3 fiber groups. Odd orders of l do not correspond to meaningful diffusion measurements and are generally assumed to be noise and artifacts.

The HARDI 3D diffusion profiles may also be modeled using generalized diffusion tensor imaging (GDTI) [9,10] which use higher order tensor statistics to model the ADC profile. The GDTI methods proposed by Liu et al. [9] demonstrate the impressive ability to model asymmetrically bounded diffusion behavior, although the method requires the accurate measurement of the signal phase, which is nearly always discarded and may be difficult to obtain in practice. One problem with these approaches is that in the case of crossing white matter tracts, the directions of maximum ADC do not necessarily correspond to the fiber directions.

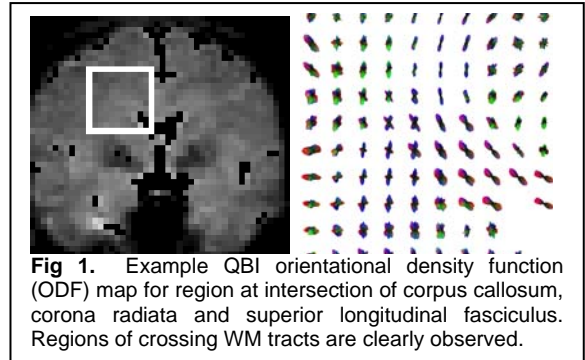


Fig 1. Example QBI orientational density function (ODF) map for region at intersection of corpus callosum, corona radiata and superior longitudinal fasciculus. Regions of crossing WM tracts are clearly observed.

One approach to this problem is the q-ball imaging (QBI) solution described by Tuch [11], which estimates the orientational distribution function (ODF) based upon the Funk-Radon Transform. According to this relationship, the ODF for a particular direction is equivalent to the circular integral about the equator perpendicular to the direction

$$\text{ODF}(\hat{r}) = \int_{q \perp \hat{r}} E(\mathbf{q}, \Delta) d^3\mathbf{q} \quad (5)$$

This integral requires that the diffusivities be interpolated over the entire surface of the sphere. Whereas the peaks in the HARDI profile do not necessarily conform to the WM tract directions, the peaks in the ODF profiles do in fact correspond to the specific WM tract direction. Since the ODF is estimated by integrating several measurements together, the SNR of the ODF will be much higher than that of the ADC values in the original HARDI.

Diffusion Spectrum Imaging (DSI): The fast/slow diffusion modeling and HARDI approaches represent

opposing approaches to complex diffusion characterization. The combination of high angular sampling at multiple levels of diffusion weighting may be used to provide information about both fast/slow diffusion and crossing WM tract orientations. The most basic approach for this application is diffusion spectrum imaging (DSI) [12] which uses diffusion-weighted samples on a Cartesian q-space lattice, where $\mathbf{q} = \gamma \mathbf{G} \delta$ is the diffusion-weighting wave-vector analogous to wave-vector \mathbf{k} used in k-space sampling for MR image acquisitions. An excellent discussion of q-space imaging is found in the text by Callaghan [13]. For a specified diffusion time, Δ , the probability distribution of diffusion displacements, $P(\mathbf{R}, \Delta)$, is related to the distribution of sampled diffusion-weighted signals in q-space, $E(\mathbf{q}, \Delta)$, through a Fourier Transform:

$$P(\mathbf{R}, \Delta) = \int E(\mathbf{q}, \Delta) e^{-i2\pi \mathbf{q} \cdot \mathbf{R}} d^3 \mathbf{q} \quad (6)$$

The derivations of q-space formalism assume that the widths of the diffusion-pulses, δ , are narrow relative to the pulse spacing, Δ , such that $\delta \ll \Delta$. The maximum gradient amplitudes on current clinical MRI systems cause this assumption to be violated for diffusion spectrum imaging, since $\delta \sim \Delta$. The effect of this will be to slightly, but consistently underestimate the diffusion displacements, and the overall distribution shape will be correct [12]. Note that relationship of DSI (q-space) to diffusion tensor imaging is that $P(\mathbf{R}, \Delta)$ is a multi-variate Gaussian (Equation (1)) and the diffusion-weighting factor is $b = |\mathbf{q}|^2 (\Delta - \delta/3)$ or $b \sim |\mathbf{q}|^2 \Delta$ for small δ . The DSI approach yields empirical estimates of the distributions of diffusion displacements (e.g., model free), which are described using the standard definitions of Fourier sampling theory. The resolution of diffusion displacements (ΔR) is defined by the range of q-space samples: $\Delta R = 1/2|q_{\max}|$; and the alias-free range of displacements $2R_{\max} = 1/\Delta q$. If the range of q-space samples is too small, then the measurement profile will be truncated, which will lead to Gibbs ringing in the reconstructed diffusion displacement spectrum. This can be ameliorated by apodization with a Hanning or Hamming window, at the cost of increased blurring of the diffusion distribution. Ideally the maximum $|q|$ should be large enough that the signal is near zero to minimize truncation effects. In adult white matter, this implies that a maximum diffusion weighting of 14,000 s/mm² or more is necessary although $b_{\max} \sim 10,000$ s/mm² are probably reasonable. A common concern with very high diffusion-weighting is that the image SNR is very low. However, the Fourier transform associated with Equation (6) will improve the SNR by the square root of the number of samples (e.g., 400 DSI samples will improve the SNR of the displacement spectra by a factor of 20). Since the distributions of diffusion displacements are model independent, the distributions may be challenging to quantify. Several features have been proposed including the zero-displacement probability, $P(\mathbf{R}=0, \Delta)$, which is higher in regions with more hindered or restricted diffusion; the mean squared displacement,

$$\text{MSD}(\Delta) = \int P(\mathbf{R}, \Delta) |\mathbf{R}|^2 d^3 \mathbf{R}, \quad (7)$$

which is related to the diffusivity; the kurtosis of the diffusion distribution, which highlights regions significant slow diffusion; and the orientational distribution function (ODF) [12]:

$$\text{ODF}(\hat{\mathbf{r}}) = \int P(\mathbf{R} \hat{\mathbf{r}}, \Delta) |\mathbf{R}|^2 dR \quad (8)$$

Note that this definition of ODF (Eq (5)) for DSI is derived differently for DSI than it is for QBI [11].

While Cartesian sampling facilitates the straightforward FFT for estimation of the displacement densities, Cartesian sampling is not required. Recently, investigators have proposed non-Cartesian sampling strategies of q-space including sampling on concentric spherical shells of constant $|q|$ [14,15]. Assaf et al. then applied a model (CHARMED) of slow and fast diffusing compartments to estimate what they deemed as hindered and restricted diffusion [14]. Wu et al. demonstrated that the concentric q-space shell samples in hybrid diffusion imaging (HYDI) could be used for DTI, DSI and QBI in the same experiment [15].

Applications of High Diffusion-Weighting: The complexity and time required to perform advanced diffusion imaging methods with high diffusion-weighting has limited the number of clinical and research studies relative to the work in diffusion tensor imaging. While studies with ~500 DW encoding measurements with b-values of 10,000 s/mm² or more may be capable of

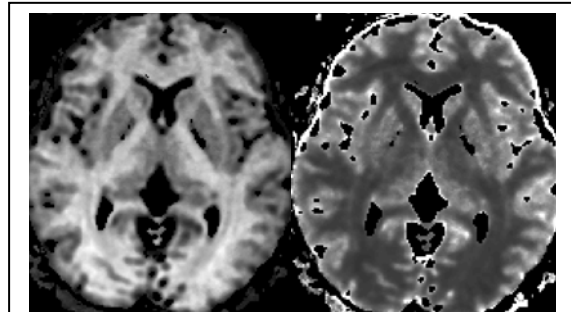


Fig 2. Example $P(\mathbf{R}=0; \Delta)$ and mean squared displacement maps from DSI study ($N_e = 257$; $b_{\max} = 9000 \text{ s/mm}^2$)

generating very interesting data on a small sample, they will not be very practical in a clinical setting unless they can provide greatly increased clinical sensitivity and specificity. Studies with ~100 DW encoding measurements are likely to be more feasible. The clinical significance of fast/slow diffusion measurements is unclear. Only one published study to date [16] has specifically examined the effects of pathology (ischemia) fast and slow diffusion components. Several small studies of hybrid DSI methods have shown promise in being sensitive to white matter changes associated with multiple sclerosis [17], autoimmune neuritis, and vascular dementia. Clearly, more studies are necessary to justify longer imaging times than DTI.

White Matter Tractography:

In addition to providing information about the mean diffusivity and anisotropy, diffusion imaging methods can also yield novel information about the orientation of local anisotropic tissue features such as bundles of white matter fascicles. In diffusion tensor imaging, the direction of the major eigenvector, \mathbf{e}_1 , is generally assumed to be parallel to the direction of white matter. This directional information can be visualized by breaking down the major eigenvector into x, y and z components, which can be represented using RGB colors – e.g., Red = \mathbf{e}_{1x} = Right/Left; Green = \mathbf{e}_{1y} = Anterior/Posterior; Blue = \mathbf{e}_{1z} = Inferior/Superior. Maps of WM tract direction can be generated by weighting the RGB color map by an anisotropy measure such as FA [18]. For many applications, the use of color labeling is useful for identifying specific WM tracts and visualizing their rough trajectories. An alternative strategy is white matter tractography (WMT), which uses the directional information from diffusion measurements to estimate the trajectories of the white matter pathways.

WMT increases the specificity of WM pathway estimates and enables the 3D visualization of these trajectories, which may be challenging using cross-sectional RGB maps.

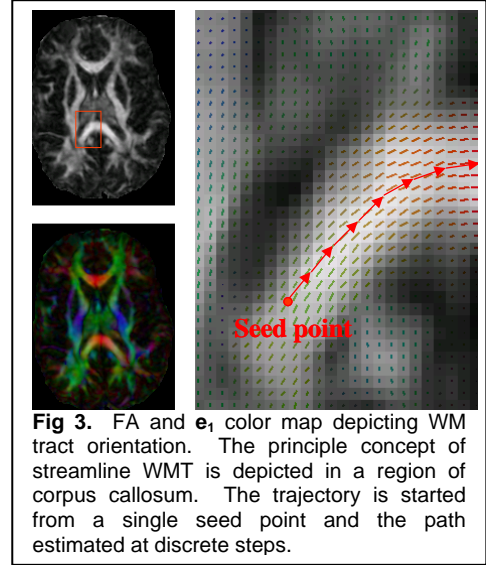


Fig 3. FA and \mathbf{e}_1 color map depicting WM tract orientation. The principle concept of streamline WMT is depicted in a region of corpus callosum. The trajectory is started from a single seed point and the path estimated at discrete steps.

Deterministic Tractography Algorithms: Most WMT algorithms estimate trajectories from a set of “seed” points. Generally, WMT algorithms may be divided into two classes of algorithms – deterministic (e.g., streamline) and probabilistic (see below). Streamline algorithms are based upon the equation:

$$d\mathbf{r} = \mathbf{v}_{\text{traj}} d\tau \quad (9)$$

where $\mathbf{r}(\tau)$ is the path and \mathbf{v}_{traj} is the vector field that defines the local path direction. Typically, streamline WMT algorithms use major eigenvector field to define the local trajectory directions $\mathbf{v}_{\text{traj}} = \mathbf{e}_1$ at each step [19-21]. Alternatively, tensor deflection (TEND) $\mathbf{v}_{\text{traj}} = \mathbf{D}\mathbf{v}_{\text{in}}$ uses the entire diffusion tensor to define the local trajectory direction [22]. The integration of deterministic pathways may be performed using simple step-wise algorithms including FACT [19] and Euler (e.g., $\Delta\mathbf{r} = \mathbf{v}_{\text{traj}} \Delta\tau$) [20] integration, or more continuous integration methods such as 2nd or 4th order Runge-Kutta [21], which enable more accurate estimates of curved tracts.

Deterministic Tractography Errors: WMT can be visually stunning. However, one significant limitation with WMT is that the errors in an estimated tract are generally unknown. Further, the visual aesthetic of WMT, which look like actual white matter patterns, can potentially instill a false sense of confidence in specific results. Unfortunately, there are many potential sources of error that can confound WMT results. Very small perturbations in the image data (i.e., noise, distortion, ghosting, etc.) may lead to significant errors in a complex tensor field such as the brain. Recent studies have shown that the dispersion in tract estimates $\langle \Delta x_j^2 \rangle$ from image noise is roughly proportional to the distance ($N \cdot w$, where N is the number of voxels and w is voxel size) and inversely proportional to the squares of the eigenvalue differences ($\Delta\lambda_j = \lambda_1 - \lambda_j$) and SNR [23,24]

$$\langle \Delta x_j^2 \rangle = N \cdot w^2 \cdot E / (\Delta\lambda_j \cdot \text{SNR})^2 \quad (10)$$

where E is a factor related to the diffusion tensor encoding scheme and the diffusion tensor orientation, and $j = 2,3$. Further, the tract dispersion is also effected by the local divergence of the tensor field [24]. Even in the complete absence of noise and image artifacts, most current WMT methods with DTI cannot accurately map WM pathways in regions with crossing fibers. New diffusion imaging methods such as

DSI and QBI described above are capable of resolving regions of white matter crossing and may ultimately improve WMT in regions of complex WM.

Probabilistic Tractography Algorithms: Although deterministic streamline algorithms are nice tools for visualizing WM patterns, they provide very little information about the reliability of specific results and are susceptible to generating highly errant results from small errors at a single step. Probabilistic tractography algorithms can overcome some of these limitations. Most probabilistic WMT algorithms are based upon some sort of iterative Monte Carlo approach where multiple trajectories are generated from the seed points with random perturbations to the trajectory directions. Model based tractography algorithms include PICo (Probability Index of Connectivity [26]), RAVE (Random Vector [27]) and ProbTrack [25]. An alternative strategy is to use bootstrap resampling to derive data-driven estimates of probabilistic tractography (e.g., BOOT-TRAC [28]). The main difference between model and data-driven approaches is that the variance of the data driven approaches will include the effects of variance in the actual data (e.g., effects of physiologic and artifact noise), not just an idealized model. All of these algorithms create a distribution of tracts, which can be used to estimate the probability of connectivity for the tractography algorithm. The connection probabilities may be used as a surrogate measure of WMT confidence. This connection probability may be used to segment structures such as the thalamus, cerebral peduncles, corpus callosum, and cortex according to patterns of maximum connectivity.

Applications of Tractography: WMT has several potential applications. (1) WMT offers the unique ability to non-invasively visualize the organization of specific WM pathways in individual subjects. To date, most studies of white matter neuroanatomy have been conducted using either anatomic dissection methods or axonal tracer studies in animals. Many recent studies have demonstrated that WMT may be used to generate tract reconstructions that are consistent with known neuroanatomy [e.g., 29-32]. However, a common criticism is that the validation of these results are missing. This concern may be addressed in two approaches – compare WMT and histopathological measurements in animal models; and develop and apply measures of WMT confidence that may be used to estimate the reliability of a specific tractography result. It should also be noted that most neuroimaging results must be interpreted without validation. (2) WMT may be used to segment specific WM pathways or portions of WM pathways. This will enable tract-specific measurements such as tract volume, cross-sectional dimensions, and the statistics of quantitative measurements within the pathways such as the mean diffusivity, and the fractional anisotropy (FA). Several studies have used WMT to perform measurements in specific WM pathways: e.g., fronto-temporal connections in schizophrenia [33]; pyramidal tract development in newborns [39], and the pyramidal tracts and corpus callosum in multiple sclerosis [34]. (3) WMT may be used to visualize specific white matter patterns relative to pathology including brain tumors, M.S. lesions, and vascular malformations. The increased specificity of WM trajectories may ultimately be useful for planning surgeries [35] as well as following the patterns of brain reorganization after surgery [36]. However, it should be noted that WMT reconstructions still need further validation before advocating its use as a tool for surgical guidance on a widespread basis. Indeed one recent study demonstrated that their WMT method underestimated the dimensions of the specific tract of interest [37]. Other studies have started to examine the relationship between specific white matter tracts affected by multiple sclerosis lesions and specific clinical impairments [38].

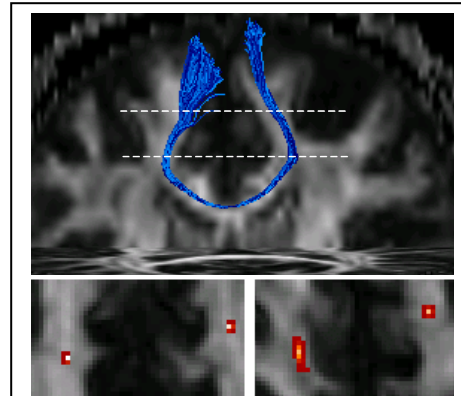


Fig 4. Probabilistic bootstrap tractography from a single seed point in the corpus callosum illustrating the tract dispersion associated with WMT at two planes above the see point. The estimated tract density or probability is shown using a hot color scale. The dispersion increases with distance from the seed.

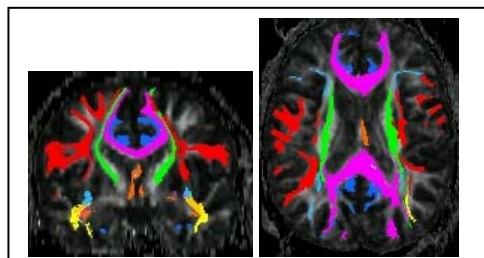


Fig 5. Parcellation of major white matter pathways using white matter tractography.

Available WMT Software Packages: This is neither a comprehensive list nor an endorsement.

| | |
|-------------------------|---|
| DTI Studio (FACT) | http://cmrm.med.jhmi.edu/ |
| FDT (ProbTrack) | http://www.fmrib.ox.ac.uk/analysis/research/fdt/ |
| TRAVIS | http://brainimaging.waisman.wisc.edu/~mlazar/TRAVIS.html |
| BioTensor (Tensorlines) | http://www.sci.utah.edu/cibc/software/index.html#biotensor |
| VtkDTMRI | http://slicer.org/vtk/Modules/vtkDTMRI/html/index.html |
| DoDTI | http://neuroimage.yonsei.ac.kr/dodti/ |
| DTI-Query | http://graphics.stanford.edu/projects/dti/dti-query/ |

References:

1. Basser PJ et al. Estimation of the effective self-DT from the NMR spin echo. *J Magn Reson B*. 1994;103:247-54.
2. Mulkern RV et al. Multi-component apparent diffusion coefficients in human brain. *NMR Biomed*. 1999;12:51-62.
3. Niendorf T et al. Biexponential diffusion attenuation in various states of brain tissue... *MRM* 1996;36(6):847-57.
4. Alexander AL et al. Analysis of partial volume effects in diffusion-tensor MRI. *MRM* 2001;45(5):770-80.
5. Maier SE et al. Biexponential diffusion tensor analysis of human brain diffusion data. *MRM* 2004;51(2):321-30.
6. Inglis BA et al. Visualization of neural tissue water compartments using biexponential DT MRI. *MRM* 2001;45(4):580-7.
7. Alexander DC et al. Detection and modeling of non-Gaussian ADC profiles... *MRM* 2002;48(2):331-40.
8. Frank LR. Characterization of anisotropy in high angular resolution DW MRI. *MRM* 2002;47(6):1083-99.
9. Liu C et al. Characterizing non-Gaussian diffusion by using generalized diffusion tensors. *MRM* 2004;51:924-37.
10. Ozarslan E, Mareci TH. Generalized diffusion tensor imaging... *MRM* 2003;50(5):955-65.
11. Tuch DS. Q-ball imaging. *MRM* 2004;52(6):1358-72.
12. Wedeen VJ et al. Mapping complex tissue architecture with diffusion spectrum MRI. *MRM* 2005;54(6):1377-86.
13. Callaghan PT. Principles of Magnetic Resonance Microscopy. Oxford University Press. (1994).
14. Assaf Y et al. New modeling and experimental framework to characterize hindered and restricted water diffusion in brain white matter. *MRM* 2004;52(5):965-78.
15. Wu YC, Alexander AL. Hybrid diffusion imaging for complex diffusion characterization. *ISMRM # 578*, 2005.
16. Brugieres P et al. Water diffusion compartmentation at high b values in ischemic human brain. *AJNR* 2004;25(5):692-8.
17. Assaf Y et al. High b-value q-space analyzed DW MRI: application to multiple sclerosis. *MRM* 2002;47:115-26.
18. Pajevic S, et al. Color schemes to represent the orientation of anisotropic tissues... *MRM* 1999;42:526-40.
19. Mori S et al. Three-dimensional tracking of axonal projections in the brain ... *Ann Neurol*. 1999;45(2):265-9.
20. Conturo TE et al. Tracking neuronal fiber pathways in the living human brain. *PNAS* 1999 31;96(18):10422-7.
21. Basser PJ et al. In vivo fiber tractography using DT-MRI data. *MRM* 2000;44(4):625-32.
22. Lazar M et al. White matter tractography using diffusion tensor deflection. *HBM* 2003;18(4):306-21.
23. Anderson AW. Theoretical analysis of the effects of noise on diffusion tensor imaging. *MRM*. 2001;46:1174-88.
24. Lazar M, Alexander AL. An error analysis of white matter tractography method... *Neuroimage*. 2003;20:1140-53.
25. Behrens TE et al. Characterization and propagation of uncertainty in DW MR imaging. *MRM* 2003;50(5):1077-88.
26. Parker GJ et al. A framework for a streamline-based probabilistic index of connectivity (PICO) *JMRI* 2003;18(2):242-54.
27. Lazar M, Alexander AL. WMT using random vector (RAVE) perturbation. *ISMRM* 539, 2002.
28. Lazar M, Alexander AL. Bootstrap white matter tractography (BOOT-TRAC). *Neuroimage*. 2005 15;24(2):524-32.
29. Stieltjes B et al. DTI and axonal tracking in the human brain. *Neuroimage* 14:723-735 (2001).
30. Catani M et al. Virtual in vivo interactive dissection of white matter fasciculi in the human brain. *Neuroimage* 17:77-94 (2002).
31. Wakana S et al. Fiber tract-based atlas of human white matter anatomy. *Radiology*. 2004 Jan;230(1):77-87.
32. Jellison BJ et al. Diffusion tensor imaging of cerebral white matter... *AJNR* 25(3):356-69 (2004)
33. Jones DK et al. Age effects on DT-MRI tractography measures of frontal cortex connections in schizophrenia. *HBM*. (in press).
34. Vaithianathar L et al. T1 relaxation time mapping of WM tracts in MS defined by DTI. *J Neurol*. 2002;249:1272-8.
35. Holodny AI et al. Tumor involvement of the CST: diffusion MR tractography ... *J Neurosurg*. 2001;95:1082.
36. Lazar M et al. White matter reorganization after surgical resection of brain neoplasms. *AJNR* (in press)
37. Kinoshita M et al. Fiber-tracking does not accurately estimate size of fiber bundle... *Neuroimage*. 2005;25(2):424-9.
38. Lin X et al. 'Importance sampling' in MS: use of DT tractography to quantify pathology related to specific impairment. *J Neurol Sci*. 2005;237:13-9.
39. Berman JI et al. Quantitative DT MRI fiber tractography of sensorimotor WM development in premature infants. *Neuroimage*. 2005;27:862-71.